Mechatronics 50 (2018) 45–54

Contents lists available at ScienceDirect

Mechatronics

journal homepage: www.elsevier.com/locate/mechatronics

A compensation approach for nonlinear gimbal axis drift of a control moment gyroscope☆

S.D. Lee, S. Jung*

Intelligent Systems and Emotional Engineering Lab., Department of Mechatronics Engineering, Chungnam National University, Daejeon, Korea

ARTICLE INFO

Keywords:
CMG
Nonlinear drift
Drift modeling and compensation
Sigmoid function

ABSTRACT

This paper investigates the axial drift phenomenon of a gimbal system of a Control Moment Gyroscope (CMG) system and proposes a solution to tackle the problem. A CMG is an indirect actuator to generate a torque in the desired direction by using a gyroscopic effect for the attitude control of dynamical systems. CMGs are easily subject to drift gradually against one direction resulting in the instability of the system. The fast repositioning control of the gimbal axis to the origin should be ensured to maximize the induced gyroscopic force. Since the position control for repositioning the gimbal axis takes time, the axial drift compensator is designed for the nonlinear drift model in the inverse dynamic control framework to shorten the repositioning time. Comparison studies with disturbance observer (DOB)-based control scheme are conducted to the same problem. Advantages and disadvantages of the proposed scheme are analysed. Experimental studies confirm that the proposed compensation method can dramatically improve the performances of the returning time to the origin and the torque regulation by compensating for the axial drift of the gimbal system compared with the conventional position control.

1. Introduction

Control moment gyroscopes (CMGs) are a torque amplifier generated from a small torque of a gimbal system [1]. The induced torques of CMGs have been used in many attitude control applications, for instance, space systems [2,3], single-wheel robot systems [4,5] and bicycle systems, underwater robot systems [6] where the direct axial actuation in the system cannot be applied to satisfy the desired motions.

CMGs in space systems such as satellites are actively used as major actuators having advantages over the propellants to change the orientation of them more accurately and faster. CMGs show more agility to change the orientation of the satellite system compared with reaction wheels. For one-wheel robots or bicycle systems, CMGs are used as a torque amplifying actuator to control the roll angle in the lateral direction, so to speak, to maintain the balance of single-wheel robot systems. The gyroscopically induced torques in one-wheel robots and bicycle systems are mainly used to maintain the balance by controlling the orientation of the system [4,5].

In the gyroscopic principle, the gyroscopic motion is induced by the cross-product of two rotational momentum of the angular velocity of the flywheel and the rotational rate of the gimbal system. The gyroscopic sensors and actuators are known to suffer from the drift due the imbalance of the mass distribution or the center of gravity of the rotational dynamics, and necessary compensation algorithms have been proposed [6–8].

For the gyroscopic actuators, the main control input to the CMGs is the rotational motion of the gimbal to generate a desired gyroscopic force and direction. Since the force is induced by two physical rotation quantities and uncertainties are present in the dynamical system, the gimbal axis tends to drift against one direction resulting in ill performance of a CMG. CMGs fall into the singular configuration with ease due to the drift problem, where CMGs do not generate a desired torque in the desired direction, leading to the null motion. Eventually this singularity of null motion leads to the instability of the body system.

Therefore, there have been many attempts to tackle the singular problem to avoid the null motion in multiple CMG configurations. One of popular approaches is the redundant configuration of adding extra CMGs to cover the null motion of a typical CMG configuration. This redundant configuration yields the multiple-single gimbal CMG(MSGCMG) or double gimbal CMG(DGCMG) structures which are complex in design and control [9–11]. The maneuverability of a SGCMG under the condition of a rapid flywheel speed change has been

☆ This paper was recommended for publication by Associate Editor Prof. T.H. Lee.

* Corresponding author.
E-mail address: jungs@cnu.ac.kr (S. Jung).
URL: http://isee.cnu.ac.kr (S. Jung).

https://doi.org/10.1016/j.mechatronics.2018.01.014
Received 16 March 2017; Received in revised form 2 January 2018; Accepted 15 January 2018
Available online 03 February 2018
0957-4158/

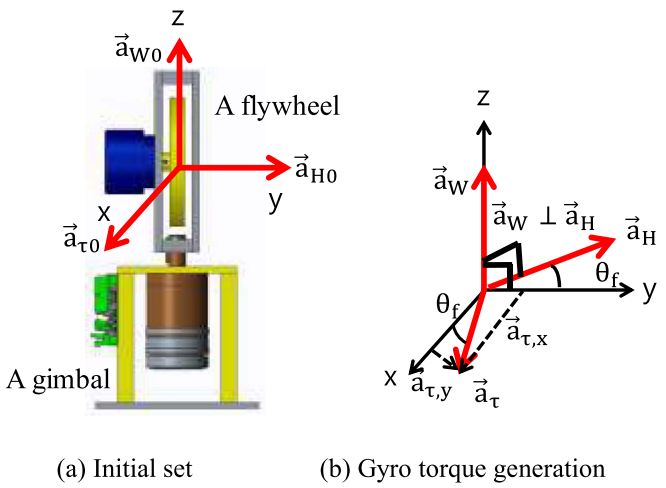

(a) Initial set (b) Gyro torque generation

Fig. 1. Configuration of single-SGCMG.

Table 1
SGCMG specifications.

Items	Values	Units
Mass of a flywheel	0.4	*Kg*
Radius of a flywheel	0.04	*m*
Moment of Inertia	0.00032	$Kg{\cdot}m^2$
Angular rate of a flywheel	628.21	*rad/s*
Angular momentum of a flywheel	0.201	*N s/rad*
Angular rate of a gimbal	9.4	*rad/s*

improved [12]. In the control point of view, the disturbance observer control method has been used to improve the performance of CMGs [13]. Singularity analysis and singularity avoidance methods have been presented for the multiple CMG configuration [14–17].

Due to the imbalance of the CMG and the fast change of the applied torque may generate an axial drift. A disturbance observer (DOB)-based current control schemes have been proposed [18]. An adaptive DOB was proposed for a robust current-control [19] and a DOB based torque control was presented [20]. However, design of DOB requires an exact inverse nominal model of the given system and an accurate design of a Q-filter.

In this paper, the singular problem caused by the axial drift of a SGCMG is remedied by a compensator design. For the motion control of CMGs, there are many causes for the axial drift such as unknown coupled dynamics between the gimbal and the body system that holds the gimbal system or between the flywheel and the gimbal system. To solve the problem, a dynamic inversion control technique with the drift compensation is proposed in the SGCMG configuration. Based on the input and output relationship of the gimbal system, the drift behavior is identified. The nonlinear axial drift can be modeled as a sigmoidal function. Parameters of the sigmoidal function are identified by the recursive least square (RLS) method. The amplitude of the sigmoidal function is represented by the angle of the gimbal, the slope by the angular rate of the gimbal, and the elapsed time by the time delay of the control.

The proposed control method is fully implemented in the real system and the performance of the proposed method is confirmed by investigating repositioning time in the current control scheme. The experimental studies demonstrate the robust-singularity free control

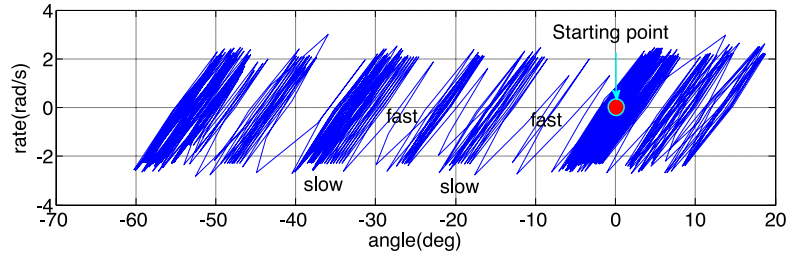

(a) Case 1: ±500mA current input

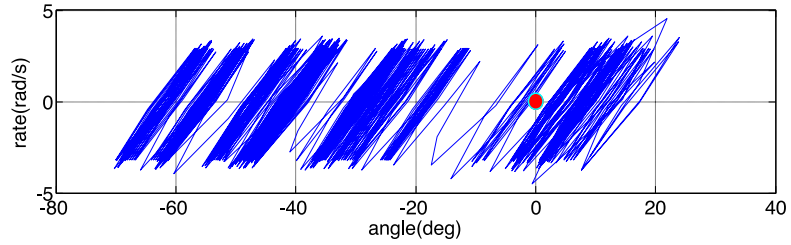

(b) Case 2: ±700mA current input

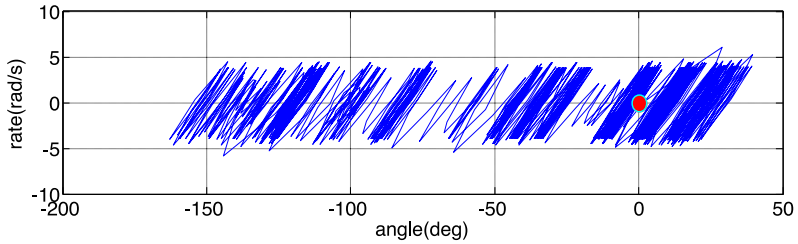

(c) Case 3: ±900mA current input

Fig. 2. Three cases of Gimbal drift phenomena.

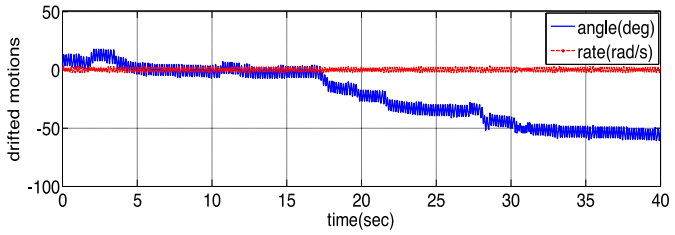

(a) Drifted motions

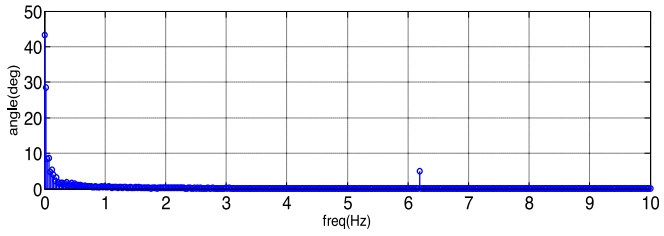

(b) Frequency characteristic

Fig. 3. Angle characteristics during the axial drift.

performances of the fast repositioning to the origin by the proposed method.

2. Control moment gyroscopes

2.1. Principle of CMG

CMGs are required to generate a regulated and directed torque for the housing systems. The direction of the induced torque can be controlled by the cross-product of the angular velocity of a flywheel mounted inside the gimbal system and the rotational rate of the gimbal system as

$$\tau = \mathbf{H} \times \mathbf{W} \tag{1}$$

where $\boldsymbol{\tau}$(Nm) is the gyroscopic torque, $\mathbf{H}$(Nm·s) is the angular momentum of a flywheel, $\mathbf{W}$(rad/s) is the angular rate of a gimbal system. Generally, the angular momentum of a flywheel is set to a constant and the angular rate of a gimbal system is used for the control purpose.

The configuration of CMG is shown in Fig. 1. It is composed of a flywheel, a flywheel motor, a gimbal motor, and control hardware. The induced torque is represented as

$$\tau = \vec{\tau}_{CMG} = \mathrm{HW}(\vec{a}_H \times \vec{a}_W) \tag{2}$$

where H is the magnitude of the angular momentum, $\vec{a}_H$ is the unit vector of the angular momentum, $\vec{\tau}_{CMG}$ is the gyroscopically induced torque through the direction change of the angular momentum, W is the magnitude of an angular rate, and $\vec{a}_W$ is the unit vector of the angular rate.

The angular momentum H can be stored in the high rotating flywheels and the speeds of them are not rapidly changed. One of the major difficulties of (2) is the control of the directional change of the gyroscopically induced torque. In (2), the direction of $\vec{\tau}_{CMG}$ can be also varied when the direction of $\vec{a}_H$ is varied.

In Fig. 1, $\vec{a}_{H0}$ is the initial direction of the angular momentum, $\vec{a}_{W0}$ is the initial direction of the gimbal axis, and $\vec{a}_{\tau 0}$ is the initial direction of the gyroscopic torque. When the gyroscopic torques are induced, their directions can be described as in Fig. 1(b). Consequently, there are two directional torques in the configuration of CMG. Two torques can be represented as

$$\vec{\tau}_{CMG} = \vec{\tau}_{CMG,x} + \vec{\tau}_{CMG,y} = \mathrm{HWcos}(\theta_f)\vec{a}_x + \mathrm{HWsin}(\theta_f)\vec{a}_y \tag{3}$$

The control purpose of the gimbal axis is to generate a regulated and directional torque. The torque direction is dependent on the angle of the gimbal axis θ_f. Due to the difficulty of direct control, SGCMG cannot exactly generate one directional torque. Nevertheless, the configuration can be available when θ_f is limited within a narrow range. To maximize the induced torque in one direction, the gimbal axis should return to its origin during the control as quickly as possible. The repositioning time is one of the performance measures of CMGs.

To achieve the better repositioning performance, the current loop control is preferred to the position loop control because the current sources are linearly proportional to the torque sources. In the framework of the current loop control, the gimbal axis drifts arbitrarily during the actuation since the system has unknown uncertainties. Therefore, the axial drift phenomenon of a gimbal system is identified and compensated for the regulated and directed torque generation in the configuration of the SGCMG.

The purpose of developing a SGCMG is to produce a 1.2 Nm gyroscopic torque. In our CMG system, the mass of the flywheel is 0.4 Kg and the radius is 0.04 m and the detailed specification is listed in Table 1.

2.2. Drift phenomenon of the gimbal axis

We have commonly observed the axial drift phenomenon of the gimbal axis in CMG controls. It is quite difficult to derive the exact dynamics of the axial drift due to the high nonlinearity. Instead of deriving a linear dynamic model, the nonlinear drift can be modeled as a sigmoidal function through the investigation of the frequency response and data fitting process by the RLS method.

To investigate the drift phenomenon, torque inputs are given to the CMG repeatedly and the corresponding outputs are checked. The position and velocity responses are plotted with respect to time. Several cases of drift phenomena at a different time span are plotted in Fig. 2. We see that the gimbal position is drifting from the original position to the certain angle as shown in Fig. 2. Those drift phenomena result in the null motion of a CMG when the deviated angle is over 45°.

To examine the characteristics of the axial drift more accurately, the axial drift phenomenon is investigated in both time and frequency

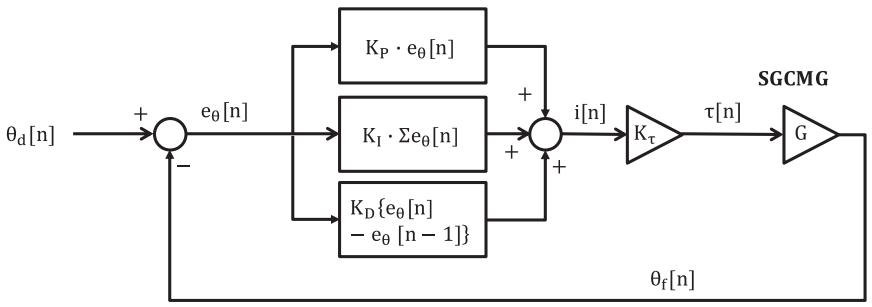

Fig. 4. Scheme 1: PID Position control block diagram.

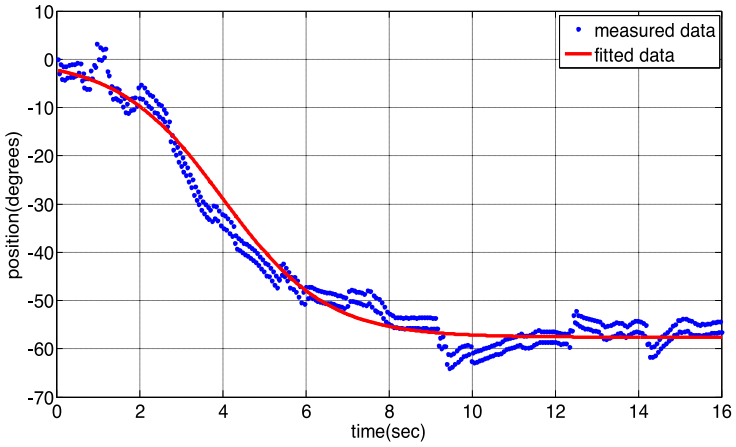

Fig. 5. Nonlinear model of gimbal drift. (For interpretation of the references to color in this figure legend, the reader is referred to the web version of this article.)

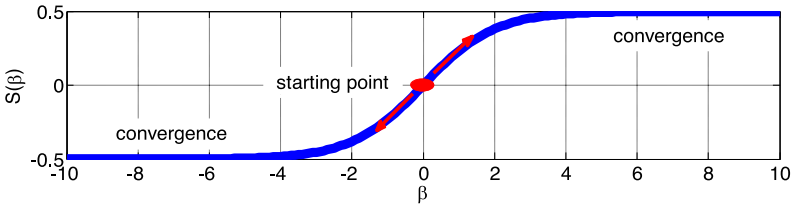

(a) Sigmoid function in the time-domain

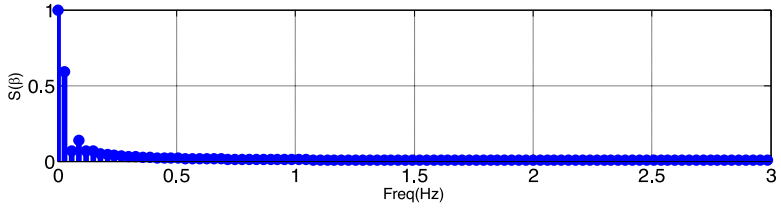

(b) Sigmoid function in the frequency-domain

Fig. 6. Drift phenomenon in time and frequency domain.

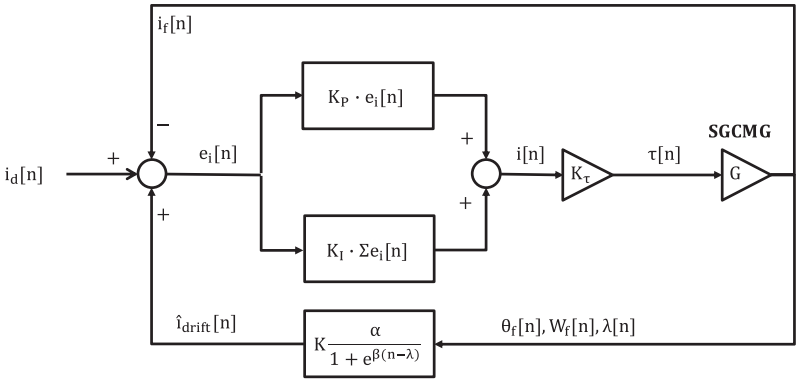

Fig. 7. Scheme 2: Proposed control block diagram.

domain as shown in Fig. 3. We see that the gimbal angle is drifting as shown in Fig. 3(a) in the time domain. From the experimental investigation of the axial drift, the drift phenomenon can be classified as low-frequency viscosity and stiffness dynamics within 1 Hz as shown in Fig. 3(b). Control frequency is around 6 Hz. This means that the drift can be decoupled in the frequency-domain when the gimbal axis has some higher switching frequencies.

Consequently, the axial drift phenomenon can be summarized for their specific characteristics as follows.

Remark: Gimbal axial drift phenomenon

- The drift has a nonlinear characteristic.
- The drift has a continuous characteristic.
- The drift has a fast moving segment and a slow moving segment.
- The drift has the feature of moving in both directions.
- The drift has a converging feature.
- The drift can be shown in the angle data and the drift can be found around 0 Hz.
- The drift can be decoupled in the frequency-domain.

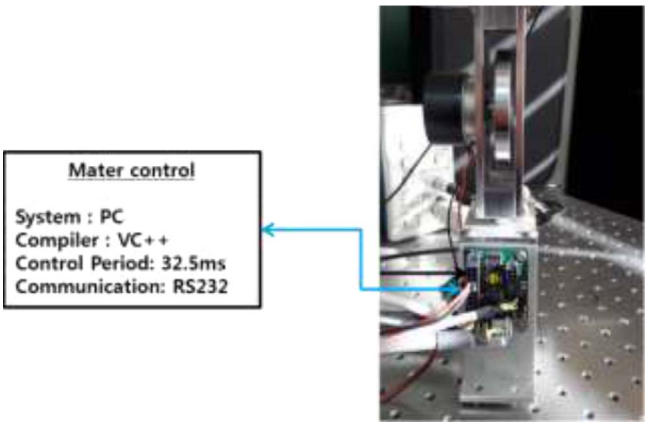

(a) Real experimental setup

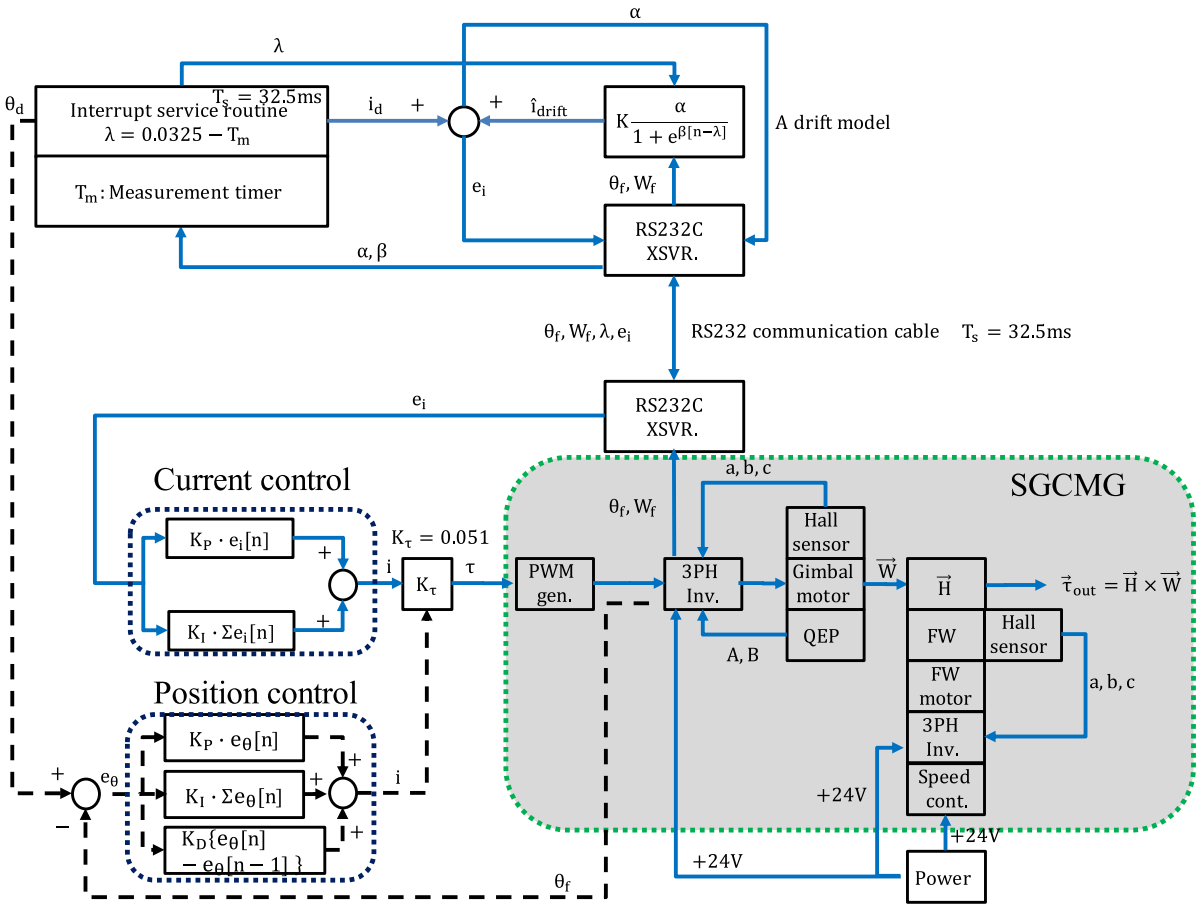

(b) Block diagram

Fig. 8. Overall control system structure.

3. Control schemes

3.1. Scheme 1: PID angle control

The position control loop can control the axial drift phenomenon of the gimbal axis. A simple PID control block diagram is shown in Fig. 4. The gimbal angle θ_f is required to track the desired angle θ_d. The tracking error is given in the discrete domain as

$$e_\theta[n] = \theta_d[n] - \theta_f[n] \tag{4}$$

where θ_d is the desired angle and θ_f is the measured gimbal angle.

The torque input becomes

$$i[n] = K_P e_\theta[n] + K_I \sum e_\theta[n] + K_D\{e_\theta[n] - e_\theta[n-1]\} \tag{5}$$

where $e_\theta[n]$ is the angle error, K_P is the proportional gain, K_I is the

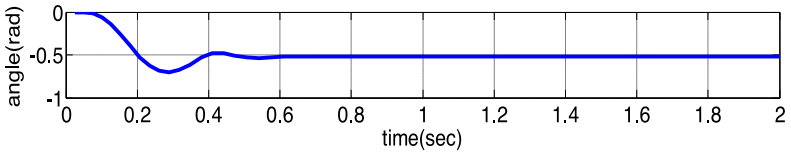

(a) Task 1

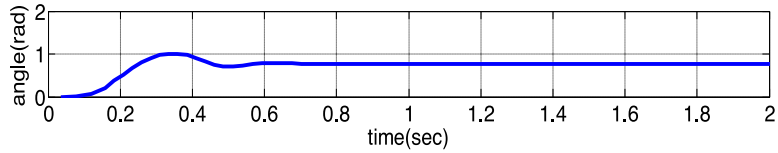

(b) Task 2

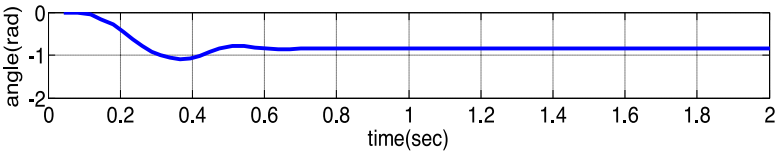

(c) Task 3

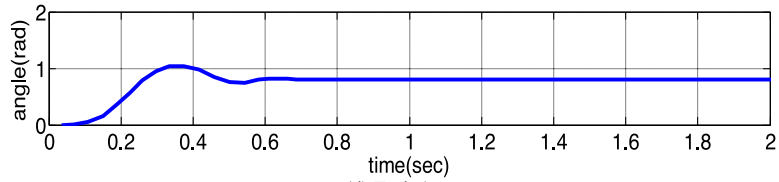

(d) Task 4

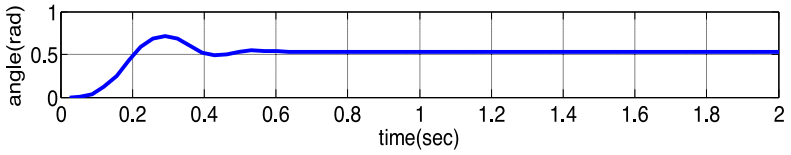

(e) Task 5

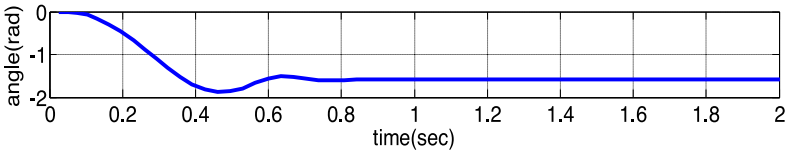

(f) Task 6

Fig. 9. Angle return performance by PID control scheme.

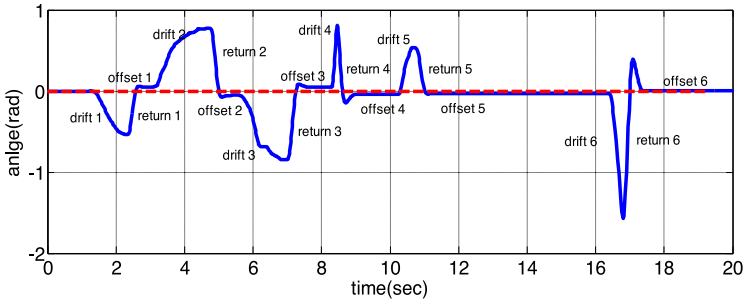

Fig. 10. Angle return performance by the proposed method.

integral gain, K_D is the derivative gain.

Compared to the proportional loop such as $K_P e_\theta[n]$, both the integral loop and current derivative loop contain numerically sophisticated calculation processes. To realize the fast process of PID control in (5), the controller requires the accuracy of feedback signals as well as the high sampling time capability.

In general, industrial servo systems have two control loops, the outer loop is for the position control and the inner loop is for the

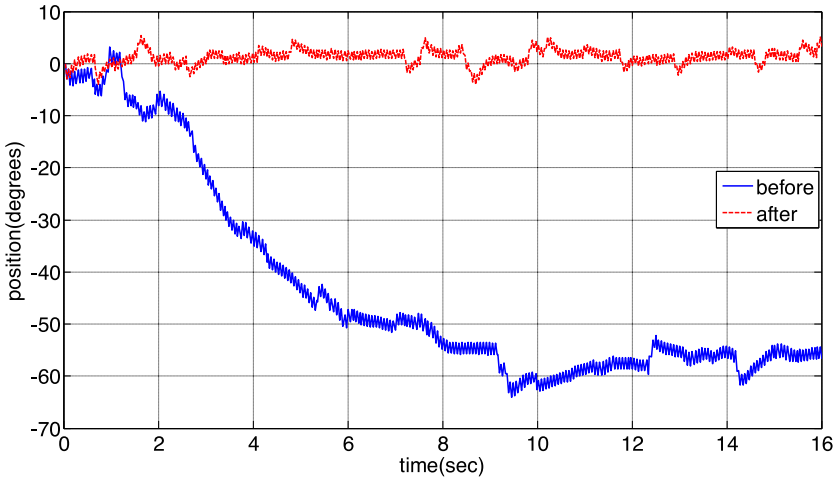

Fig. 11. Gimbal position before and after compensation. (For interpretation of the references to color in this figure legend, the reader is referred to the web version of this article.)

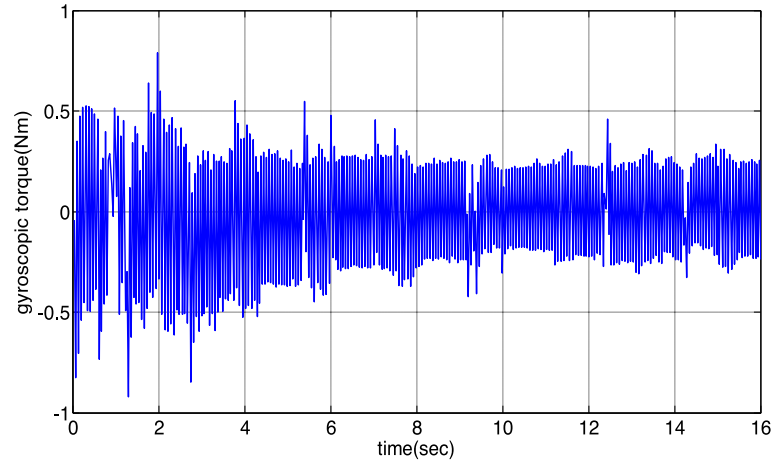

(a) Before compensation

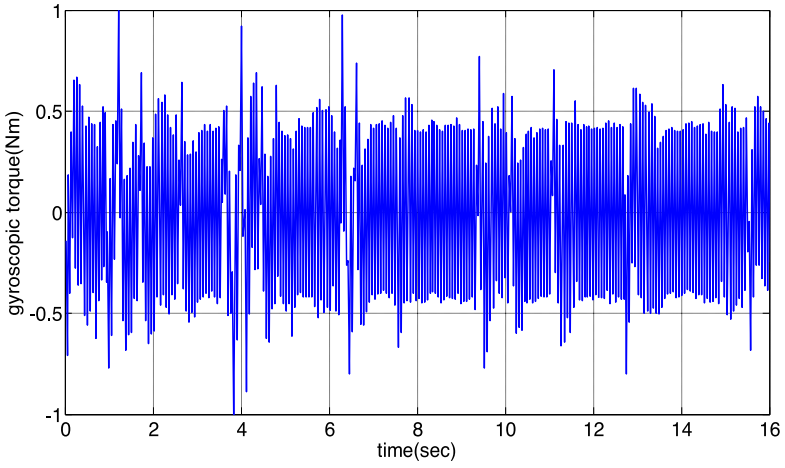

(b) After compensation

Fig. 12. Gyroscopic torque comparison.

current control. The inner loop current controller typically has over 10 times wider bandwidth than that of the outer loop. Consequently, the current control loop is adopted for the agile control of the gimbal motion of a SGCMG. In the experimental verification, the drift compensating performance of the current control loop can be compared to that of the position control loop.

3.2. Scheme 2: control schemes for drift compensation

3.2.1. Identification of axial drift

To maximize the gyroscopic effect of the housing systems, the gimbal should return to the initial angle (e.g. zero degree) rapidly as control time goes. However, in real applications such as balancing control of a single wheel robot [4], the gimbal angle drifts with respect

Table 2
Performance comparison between two schemes.

Tasks	Drift(rad)	Return time(s) by Scheme 1	Return time(s) by Proposed Scheme 2
1	−0.52	0.57	0.34
2	0.77	0.62	0.29
3	−0.84	0.60	0.45
4	0.80	0.64	0.30
5	0.53	0.60	0.34
6	−1.574	0.79	0.63

to time and results in angle deviation, even in instability of the robot system as shown in Fig. 5. The gimbal angle drifts to 60° from the initial angle. This causes the null motion of CMG.

To remedy this problem, a nonlinear drift model of the gimbal axis is identified by the off-line recursive least square (RLS) method. Models are obtained based on input and output data when the torque current inputs of ± 800mA are applied to the gimbal motor repeatedly. The corresponding plot from the current input and the gimbal angle output for 16 seconds is shown in Fig. 5. The measured angle data shown as a blue dotted line drift away from the initial zero angle as time goes. The corresponding approximation is plotted as a red solid line together to estimate the nonlinear drift model.

We can easily notice that the drift model is similar to a sigmoidal function shown in Fig. 6(a). The corresponding frequency characteristic of the drift is shown in Fig. 6. (b), which shows the low frequency characteristics, which is similar to Fig. 3(b).

The characteristics of the gimbal axial drift are similar to a sigmoidal function. The sigmoidal function has a nonlinear and continuous characteristic. In addition, the frequency characteristic of the sigmoidal function is similar to that of the gimbal axial drift as shown in Fig. 6.

From Figs. 5 and 6, the sigmoidal function of the axial drift model becomes

$$\tau_{\text{drift}} = \frac{\alpha}{1 + e^{\beta(n-\lambda)}}, \quad \alpha = \text{angle}, \quad \beta = \text{velocity}, \lambda = \text{time delay} \tag{6}$$

The parameters of the sigmoidal function in (6) can be changed with current states of data at every sampling time in the control law.

3.2.2. The proposed compensator design

The proposed control scheme is described in Fig. 7. A torque drift model is added to the PI current control for the gimbal motor to cancel the drift torque. The equation of CMG is given as follows.

$$I\dot{W}[n] + BW[n] + K_{\text{stiff}}\theta_f[n] + \tau_{\text{drift}}[n] = \tau[n] + \hat{\tau}_{\text{drift}}$$
$$= \tau[n] - 0.051\hat{i}_{\text{drift}}[n] \tag{7}$$

where I is the moment of inertia, B is the damping, K_{stiff} is the stiffness, θ_f is the gimbal angle, W is the angular velocity of the gimbal, τ is the input control torque and τ_{drift} is the drifted torque, $\hat{\tau}_{\text{drift}}$ is the drift model, −0.051 is the current to torque conversion factor, and $\hat{i}_{\text{drift}}$ is the drift compensating current.

From Fig. 7, the current error is defined as

$$e_i[n] = i_d[n] - i_{fb}[n] + \hat{i}_{\text{drift}}[n] \tag{8}$$

where $i_d[n]$ is the current input and $i_{fb}[n]$ is the current feedback. The drift compensating current $\hat{i}_{\text{drfit}}[n]$ can be estimated as a sigmoidal function.

$$\hat{i}_{\text{drift}}[n] = K\hat{\theta}_f = K\frac{\alpha[n]}{1 + e^{\beta[n](n-\lambda[n])}} \tag{9}$$

where $\alpha[n]$ is the angle of the gimbal system, $\beta[n]$ is the angular velocity of the gimbal system, $\lambda[n]$ is the time delay of the control, $\hat{\theta}_f[n]$ is the estimated drift, and K is the angle to current conversion constant which is 0.2. The parameters of the axial drift model such as $\alpha[n]$, $\beta[n]$, and $\lambda[n]$ are changed at every sampling time. The time delay parameter $\lambda[n]$ is to shift the sigmoid function to exactly compensate for the exhausted time between the measured time and the compensation time. In the control program, we have used a hardware tick counter to find out the value.

The PI control as inner loop control is given as

$$\tau[n] = K_\tau i[n] = K_\tau(K_P e_i[n] + K_I \sum e_i[n]) \tag{10}$$

where K_P is 1811, K_I is 366, and K_τ is a torque constant of 0.051(Nm/A).

To construct the parameters such as $\alpha[n]$, $\beta[n]$, and $\lambda[n]$ are the angle, angular velocity, and the time delay of the control can be used.

4. Experimental verification

4.1. Experimental setup

To validate the proposed control method, experiments are conducted and the experimental set up is described in Fig. 8(a). The detailed block diagram of the experimental setup is shown in Fig. 8(b). The PI torque controller for the gimbal is connected with the host controller of a PC using RS232 communication, and written in VC++ Software. The PID position control block can be used by replacing the PI torque control block. The overall control execution time is 32.5 ms.

When the measured data $\alpha[n]$, $\beta[n]$ are received via RS232C XSVR (Transmitter and receiver), the hardware tick count method checks the time delay $\lambda[n]$ and the delay is transmitted into the axial drift model. During a cycle of ISR (Interrupt Service Routine), a new desired current value is calculated and the drift compensated current error is transmitted to the controller. The PI controller calculates the control output with the received error. After the PI control process, the command

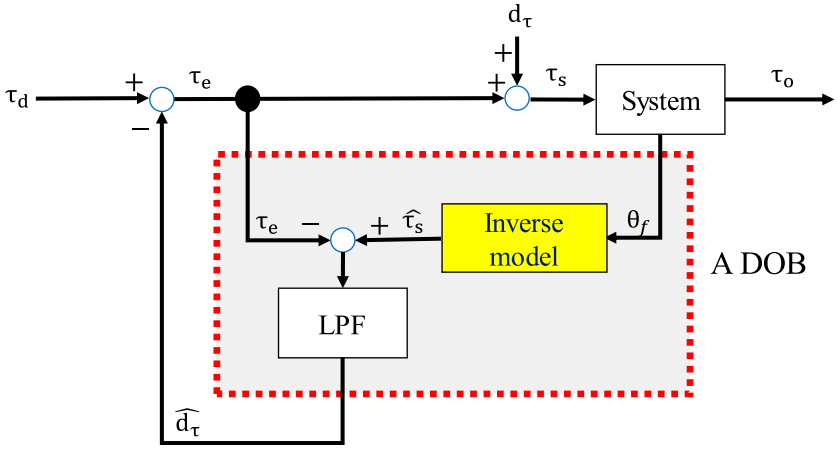

Fig. 13. DOB scheme.

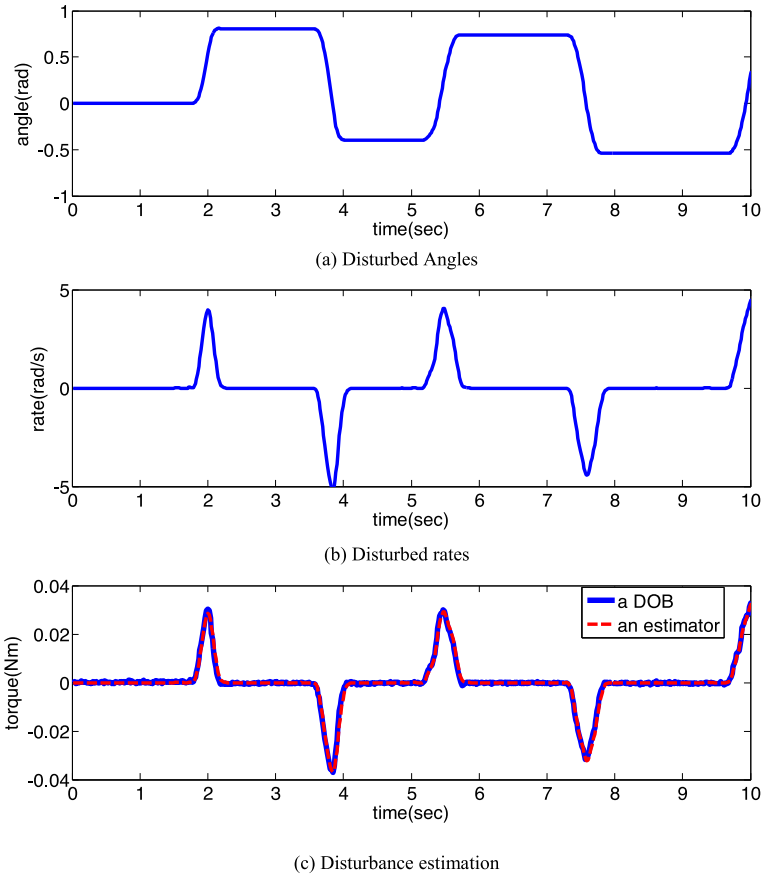

(a) Disturbed Angles

(b) Disturbed rates

(c) Disturbance estimation

Fig. 14. Disturbance torque estimation.

Table 3
Comparison between the DOB and the proposed estimator method.

Properties	DOB	Axial drift estimator
Model property	A linear	A nonlinear
Implementation	Complex	Simple
Advantage	Wide bandwidth	Fast response
Disadvantage	A lag	Narrow bandwidth

current value is converted into the torque quantity.

The input current $i_d[n]$ drives the 3-phase inverter to produce the current step through 6-step phase switching logic to move the blushless dc motor and the gimbal motor. In the flywheel system, a speed controller is integrated in the package of the motor system. CMG can generate a gyroscopic torque by the cross product between the angular momentum vector and the gimbal motion vector. In the experiment, ISR is programmed to alter the direction of the same quantity of currents repeatedly so that it can generate a discrete torque pulse. The axial drift compensation effect can be seen more clearly.

Experiments for two schemes are conducted and their performances are compared. The axial drift compensation capability and the torque regulation capability are investigated.

4.2. Scheme 1: PID control

Firstly, a conventional PID position controller is adopted and their gains are automatically selected with the help of the Maxon motor drive utility program. The PID-gains are selected as 150, 10, and 200, respectively. The six experiments are conducted and the results are shown in Fig. 9.

4.3. Scheme 2: drift compensation scheme

The performance of the proposed scheme 2 is shown in Fig. 10. Fig. 10 shows the drift phenomena of the gimbal axis, and the corresponding compensation to make the gimbal axis return to the original position.

Experimental results of the gimbal axis are shown in Fig. 11. The gimbal axis is drifting and converged around 60° as time goes when the compensation technique is not applied (blue solid line). In the meanwhile, the gimbal axis does not deviate from the initial angle (e.g. zero) after the proposed compensation technique is applied (red dotted line). We see clearly the better repositioning performance without drifting by the proposed control scheme 2.

The corresponding induced torques are also plotted in Fig. 12 to ensure the improvement of the induced torque by the torque regulation of the proposal. The induced torque before compensation is initially about 0.5 N, but gradually reduced to a half as shown in Fig. 12(a). However, for the compensation case, we clearly see that the induced torque after compensation is uniform and well regulated from the beginning to the end. The induced torque is about double of that before the compensation. These results clearly demonstrate the better performance by the proposed compensation technique.

Performance comparison of the return time between two control schemes is listed in Table 2. The gimbal axis successfully returns to the original position by both control schemes. However, we clearly see that the proposed scheme 2 shows the faster return performances, which is about 2 times faster than those of scheme 1. This means that the effectiveness of the induced torque of scheme2 is much higher.

4.4. Comparison with a DOB scheme

The proposed method is further verified by comparing with a DOB. To implement DOS scheme, we need an inverse model of the system.

Here the model as a second-order proper function has been identified by a RLS method based on random input-output data relationship.

The identified system model of the given system is

$$G^{-1}(z) = -81.09\frac{0.001593 - 0.001313z^{-1} - 0.0002631z^{-2}}{1 + 0.9992z^{-1} + 0.000007z^{-2}} \quad (11)$$

The DOB control structure is shown in Fig. 13. The purpose of the DOB is to identify the disturbance d_τ and cancel it out. In Fig. 13, τ_d is a torque input, τ_e is a torque error, d_τ is a disturbance, τ_s is a system input torque, τ_o is a system output torque, $\hat{\tau}_s$ is an estimated torque, $\hat{d}_\tau$ is an estimated disturbance, θ_f is an angle, W_f is a rate, and λ is a time delay.

We investigate the proposed method by comparing the performance with that of the conventional DOB. The experiments are conducted by giving intentional disturbances to the system. Control performances of estimating the disturbed torque are compared. Fig. 14(c) shows the comparison results between the proposed estimator and the DOB. The estimated torques by two methods are quite similar when compared with Fig. 14(b). This means that two methods compensate successfully for the axial drift problems of CMG.

In Fig. 14, two methods could successfully estimate the intentionally applied disturbances. Based on the experimental studies, we could compare the overall properties between the conventional DOB and the axial drift estimator as listed in Table 3.

5. Conclusions

The nonlinear torque drift model was identified by the recursive least square method through input and output relationship of the CMG. Based on the identified sigmoidal model, a new compensation technique for the torque control of the gimbal axis in CMG was presented. Experimental results showed that the induced torque becomes uniform without the gimbal axis drifting by the proposed compensation method. The gyro torque amplification as well as the regulation performance has been improved. We have confirmed the faster angle return performance by the proposed drift compensation method. The cancellation by the nonlinear drift model identified by the RLS method actually prevents the gimbal from deviating away from the origin. Although comparing the experimental results between the drift estimator and DOB scheme shows the comparable performances, the proposed method can be implemented with ease. Since the proposed method results in the improvement of the induced torque, it can be applied to multiple configuration of CMGs as well.

Acknowledgment

The authors would like to thank all the reviewers for their valuable comments. This research has been supported by the basic research program of National Research Foundation of Korea (2016 R1A2B2012031).

References

[1] Lappas V, Steyn W, Underwood C. Torque amplification of control moment gyros. Electron Lett 2002;38(15):837–9.
[2] Bishop RH, Paynter SJ, Sunkel JW. Adaptive control of space station with control moment gyros. IEEE Control Syst 1992:23–8.
[3] Gui H, Yukovich G, Xu S. Attitude tracking of a rigid spacecraft using two internal torques. IEEE Trans Aerospace Electron Syst 2015;51(4):2900–14.
[4] Park JH, Jung S. Development and control of a single-wheel robot: practical mechatronics approach. Mechatronics 2013;23:594–606.
[5] Zhu Y, Gao Y, Xu C, Zhao J, Jin H, Lee J. Adaptive control of gyroscopically stabilized pendulum and its application to a single-wheel pendulum robot. IEEE/ASME Trans Mechatron 2015;20(5):2095–106.
[6] Gollomp B. Gyroscopes. IEEE Instrum Meas Mag 2001;4(3):49–52.
[7] Georgy J, Noureldin A, Korenberg M, Bayoumi M. Modelling the stochastic drift of a mems-based gyroscope in Gyro/Odometer/GPS integrated navigation. IEEE Trans Intell Transp Syst 2010;11(4):852–72.
[8] Aktakka E, Woo J, Egert D, Gordenker J, Najafi K. A microactuation and sensing platform with active lockdown for in situ calibration of scale factor drifts in dual-axis gyroscopes. IEEE/ASME Trans Mechatron 2015;20(2):934–43.
[9] Thornton B, Ura T, Nose Y, Turnock S. Zero-G class underwater robots: unrestricted attitude control using control moment gyros. IEEE J Ocean Eng 2007;32(3):565–83.
[10] Berry A, Lemus D, Babuska R, Vallery H. Directional singularity-robust torque control for gyroscopic actuators. IEEE/ASME Trans Mechatron 2016;21(6):2755–63.
[11] van Wingerden JW, Hulskamp A, Barlas T, Houtzager I, Bersee H, van Kuik G, Verhaegen M. Two-degree-of-freedom active vibration control of a prototyped “Smart” rotor. IEEE Trans Control Syst Technol 2010:284–96.
[12] Jikuya I, Fujii K, Yamada K. Attitude maneuver of spacecraft with a variable-speed double gimbal control moment gyro. Adv Space Res 2016;58(7):1303–17.
[13] Leve FA. Evaluation of steering algorithm optimality for single-gimbal control moment gyroscopes. IEEE Trans Control Syst Technol 2014;22(3):1130–4.
[14] Schaub H, Junkins JL. Singularity avoidance using null motion and variable-speed control moment gyros. J Guidance Control Dyn 2000;23(1):11–6.
[15] Bedrossian NS, Paradiso EV, Bergmann EV, Rowell D. Redundant single gimbal control moment gyroscope singularity analysis. J Guidance Control Dyn 1990;13(9):1096–101.
[16] Wie B. Singularity escape/avoidance steering logic for control moment gyro systems. J Guidance Control Dyn 2005;28(5):948–56.
[17] Wie B. Singularity analysis and visualization for single-gimbal control moment gyro systems. J Guidance Control Dyn 2004;27(2):271–82.
[18] Sun JJ, Peng C. Disturbance observer control method in DGMSCMG. Electron Lett 2014;50(14):989–90.
[19] Abdel-Rady Y, Mohamed I. Design and implementation of a robust current-control scheme for a PMSM vector drive with a simple adaptive disturbance observer. IEEE Trans Ind Electron 2007;54(4):1981–8.
[20] Murakami T, Yu F, Ohnishi K. Torque sensorless control in multi-degrees-of-freedom manipulator. IEEE Trans Ind Electron 1993;40(2):259–65.